Journal of Environmental Chemical Engineering 10 (2022) 108190

Contents lists available at ScienceDirect

Journal of Environmental Chemical Engineering

journal homepage: www.elsevier.com/locate/jece

The fate and dynamics of iron during the transformation of activated sludge into oxygenic photogranules (OPGs) under hydrodynamic batch conditions for environmental applications

Abeera A. Ansari [a,b,*], Arfa A. Ansari [a], Asif Hussain Khoja [b], Gitau J. Gikonyo [a], Ahmed S. Abouhend [a], Chul Park [a]

[a] Department of Civil and Environmental Engineering, University of Massachusetts, Amherst, MA 01002, USA
[b] U.S-Pakistan Center for Advanced Studies in Energy (USPCAS-E), National University of Sciences and Technology (NUST), Sector H-12, Islamabad 44000, Pakistan

ARTICLE INFO

Editor: Fumitake Takahashi

Keywords:
Oxygenic photogranules
Hydrodynamic batch cultivation
Cyanobacteria
Activated sludge
Wastewater treatment

ABSTRACT

Oxygenic photogranules (OPGs) are dense, spherical structures containing filamentous cyanobacteria, microalgae, and non-phototrophic bacteria. Besides hydrostatic batch conditions, OPGs can be produced directly from activated sludge under illuminated hydrodynamic batch conditions. The role of Fe in these hydrodynamic batch conditions is still unknown. In this study, four replicate hydrodynamic batches with two times diluted Amherst and Hadley activated sludges were operated under continuous illumination (126 ± 9 μmol/m^2-s) and mixing (20 rpm) for a period of 19 days. Illumination and initial anaerobic condition development led to the rapid release of Fe, especially Fe (II), into the bulk liquids. However, this Fe pool quickly declined and remained at overall steady values. The Fe linked with biomass-bound extracellular polymeric substances (bEPS-Fe) continued to decline during batches and eventually reached stable levels. Cyanobacterial growth exhibited moderate to strong negative correlations to both bEPS and bulk-liquid Fe pools whereas microalgal growth showed more dependence on bulk-liquid Fe compared to bEPS-Fe. The Fe distribution analysis revealed higher Fe content in the biomass pellet fraction, followed by bEPS extract and bulk liquid fraction. Increases in the level of pelletized Fe, over the course of photogranulation, are likely due to increases in intracellular Fe content. Overall, the study demonstrates that the limitation of available Fe in bEPS and bulk liquid fractions encouraged the formation of photogranules in hydrodynamic batch conditions. These observations are similar to earlier reported batch hydrostatic cultivation, which further supports the shared photogranulation phenomena in the two batch conditions.

1. Introduction

The traditional wastewater treatment process has been around for decades, however, it still faces various sustainability challenges. A key issue, among them, is reliance on external aeration during the biological treatment stage, which currently has the highest energy demand in the wastewater treatment process [1,2]. Another major concern is the release of greenhouse gas emissions during the biological treatment process [3]. There is a need for a green, cost-effective wastewater treatment process, which could promote sustainable development of the world.

Recently, a new wastewater treatment technology namely oxygenic photogranules (OPG) has been introduced to address these challenges. OPGs are dense spherical structures having motile filamentous cyanobacteria that enclose other bacteria and microalgae in a granular aggregate [1,4–6]. These OPGs result from the transformation of activated sludge inoculum under hydrostatic conditions in the presence of an illumination source [4,5,7]. The hydrostatically-produced OPGs are then utilized as seeds in hydrodynamically operated bioreactors for the rapid start-up of OPG-based wastewater treatment processes [1,4,8]. The OPGs generated during the operation of the bioreactor share similar granular morphology with the seed biomass. The presence of phototrophs enables OPG-based processes to treat wastewater without external aeration. The OPG's ability to self-aerate via photosynthetic

* Corresponding author at: U.S-Pakistan Center for Advanced Studies in Energy (USPCAS-E), National University of Sciences and Technology (NUST), Sector H-12, Islamabad 44000, Pakistan.
E-mail address: abeera@uspcase.nust.edu.pk (A.A. Ansari).

https://doi.org/10.1016/j.jece.2022.108190
Received 24 December 2021; Received in revised form 20 June 2022; Accepted 29 June 2022
Available online 1 July 2022

oxygenation, fix carbon, and settle rapidly in water makes OPG-based systems a promising green environmental biotechnology for the treatment of wastewater [1,2,4,8].

Recently Ansari et al. [9] investigated the role of iron (Fe) in the formation of OPGs under hydrostatic cultivations. Fe is an essential micronutrient which is involved in numerous cellular processes, such as photosynthesis, respiration, photopigment synthesis, nitrogen fixation and assimilation [10–12]. Among the microbial community, cyanobacteria, the key granulating microbes in OPGs [4], have exceptionally high Fe requirements for their metabolic activities [12–16]. Studies have reported that cyanobacteria form colonies/aggregates under Fe limitations. Ansari et al. made similar observations in an OPG study that the limitation of the available Fe pool drove the cyanobacteria to aggregate and ultimately form spherical-like OPGs. Cyanobacterial growth showed a strong negative correlation with Fe linked with biomass-bound extracellular polymeric substances (bEPS-Fe), and they reached the stationary growth phase when bEPS-Fe levels also significantly decreased and became constant. Ansari et al. [9] further reported the presence of insoluble Fe(III) oxides within the photogranular biomass, which is known to bind EPS and promote granulation as a bio-coagulant [17]. These findings, hence, demonstrate Fe as a potential driving force in the formation of OPG in a hydrostatic environment.

Previously, Gikonyo et al. [18] revealed the direct production of OPGs from activated sludge under hydrodynamic batch conditions. The practical outcome of this study was to find a way to begin the OPG-based system faster than the previous method, which depended on the hydrostatically formed OPG as a seed biomass. This study concluded that, although conditions in which OPGs are produced are substantially different between hydrostatic and hydrodynamic batches, the formation is generally based on the same phenomenon as the morphological and physio-chemical characteristics of OPGs from the two sources are very similar. The question then arises: *does the limitation of available Fe, as seen in hydrostatic batches, also occur and influence the OPG formation in hydrodynamic batches?*

The present study examined the above research question by operating replicate hydrodynamic batches using two different sources of activated sludge. The hydrodynamic batches used one combination of light intensity, seeding density, and mixing conditions, which previously showed the formation of OPGs [18]. Fe content in bulk liquid, extracted bEPS, and whole biomass was determined at regular time intervals throughout the cultivation. The size distribution and oxidation states of Fe in the bulk liquid were also studied. Additionally, this study investigated the growth of different phototrophic communities and their relationship with the available Fe pool during the course of photogranulation. The outcome of this study is expected to help to better understand the photogranulation phenomenon, which seems to occur in widely varying environments [19]. The acquired knowledge will encourage the successful application of OPGs, thereby treating wastewater in sustainable ways.

2. Materials and method

2.1. Batch setup and operation

Hydrodynamic batch cultivation was conducted by using a coagulation jar setup (Phipps and Bird jar tester, model 7790302, USA) for the duration of 19 days. Prior to the experiment, activated sludges were collected from the aeration basins of wastewater treatment plants (WWTP) in Amherst and Hadley, MA, USA, with operational schemes as documented by Kuo-Dahab et al. [5]. These sludges were diluted two times with distilled water in a 1:1 ratio. An appropriate dilution factor was selected using the Gikonyo et al. [18] study on hydrodynamic cultivation of OPGs. The dilution of inoculum is reportedly anchored on substrate microbial balance, i.e., food to microorganism (F:M) metric, where the substrates 'food' are nutrients, light and shear. The selected dilution ratio increased the light attenuation, as per Beer-Lamberts Law, lowered drag during mixing, and subsequently enhanced the nutrient consumption to bring about a rapid onset of a feast-famine condition, which is a prerequisite for photogranulation [18]. The dilute matrix also exhibits fewer inter-particle collisions, thereby preserving the OPG bio-aggregate [18].

Eight hundred (800) mL of diluted activated sludge was incubated in four replicates of 1.0 L batches. These batches were mixed at 20 rpm using a straight blade stainless-steel impeller (5 cm diameter). The mixing speed was based on a previous study where high shear conditions were found to inhibit the granulation process, especially OPGs [18]. The batches received continuous light intensity of 126 ± 9 μmol/m^2-s using 9 W LED bulbs (EcoSmart, daylight-5000 K). The application of continuous illumination, through an artificial source, resulted from the subsequent engineering of the OPG process to improve its efficacy and reduce the granulation period [5,9,18,20]. The experimental setup was undertaken at a constant room temperature of 18 °C. Triplicate composite samples were prepared at each sampling point by combining known volumes of mixed biomass samples from all four batches.

2.2. Analysis of the fate and dynamics of Fe over the course of cultivation

The Fe content in bulk liquid, extracted biomass-bound extracellular polymeric substances (bEPS) and the whole biomass was determined at different sampling points during the course of this study. The Fe content was analyzed in two bulk liquid size fractions, namely colloidal (0.45 μm – 30 kDa) and dissolved (<30 kDa) phases. In brief, the bulk liquid was passed through a 0.45 μm mixed cellulose ester membrane (Fisher Scientific, USA). The obtained filtrate comprised of both colloidal and dissolved Fe fractions. The Bulk liquid was also passed through a 30 kDa membrane (ultra-filtration membrane, EMD Millipore Corporation, Billerica, MA, USA) which was considered as the dissolved Fe fraction [21]. The Fe difference in the 0.45 μm and 30 kDa filtrates was defined as the colloidal Fe. These bulk liquid filtrates were immediately acidified with concentrated trace metal grade HNO_3 (2 % by vol) (Fisher Scientific, USA) and stored in a 15 mL falcon tube at 4 °C till further analysis.

The bEPS-Fe was determined after extracting bEPS from the composite samples using sequential sonication and base treatment method [8]. The 10 mL of composite sample was subjected to centrifugation at 12,000 rpm for 10 min. The resulting supernatant was discarded and replaced with a 5 mL phosphate buffer solution (10 mM NaCl, 1.2 mM KH_2PO_4, and 6 mM Na_2HPO_4). These samples were then homogenized at 700 rpm for 30 s (IKA T18 basic Ultra-Turrax), followed by sonication (Fisher Scientific Sonic Dismembrator Model 500) at 10 % strength for 40 s and centrifuged at 12,000 rpm for 10 min. The resulting supernatant was filtered through a 0.45 μm cellulose filter. This filtrate was then considered as bEPS extract via sonication treatment. The remaining pellet was re-suspended in a 5 mL phosphate buffer solution and its pH was increased to 10.5–11 using 1 M NaOH [22]. These samples were placed on a shaker for 2 hr at 425 rpm in a 4 °C constant temperature room. After centrifugation, the resulting supernatant was filtered through a 0.45 μm cellulose filter to obtain the bEPS extract via base treatment [22]. After each treatment, the bEPS extracts were acidified with concentrated trace metal grade HNO_3 (2 % by vol) before storing at 4 °C till further analysis. The total bEPS-Fe was the summation of the Fe content in the sonic and base-treated bEPS extracts. The whole biomass Fe quantity was determined after subjecting 10 mL of a composite sample to acid-digestion per Standard Methods (3030 E)[23]. The Fe concentrations in the acidified bEPS extracts, bulk liquid fractions, and whole biomass digest samples were determined using inductively coupled plasma mass spectrometry (ICP-MS, Perkin-Elmer SCIEX). The pellet Fe was calculated by subtracting bEPS-Fe (0.45 μm) and bulk-liquid Fe (0.45 μm) from the whole biomass Fe.

Besides the total Fe concentration, the oxidation states of Fe in different bulk liquid fractions were determined using the Ferrozine method [24]. Ferrozine is a strong Fe(II) chelator that forms a magenta-colored Fe-$(FZ)_3$ complex with Fe(II) [25]. The Fe(II)

absorbance was read at 562 nm using a spectrophotometer (DR 2700 portable, Hach, USA), which was later quantified using ferrous ammonium sulfate standards. The concentrations of Fe(III) were obtained by subtracting bulk-liquid Fe(II) from total bulk-liquid Fe concentrations.

2.3. Analytical measurements

General analytical parameters, such as total solids (TS), chlorophyll content and sludge volume index (SVI) were regularly determined using Standard Methods [23]. The Phycobilin content in photogranular biomass was determined after modifying protocols by Bennett and Bogorad [26] and Islam et al. [27]. In brief, 10 mL of a composite biomass sample was centrifuged at 12,000 rpm for 10 min. The obtained supernatant was discarded and replaced with 5 mL of a 0.025 M phosphate buffer saline solution (pH 7.2). The sample was then homogenized (IKA T18 basic Ultra-Turrax) at 700 rpm for 1 min and sonicated (Fisher Scientific Sonic Dismembrator Model 500) at 20 % strength for 2 min. After treatment, the sample was centrifuged, and its resulting supernatant was passed through a 0.22 μm syringe filter (Basix, Fisher Scientific) prior to absorbance reading. The absorbance for phycoerythrin (PE), phycocyanin (PC) and allophycocyanin (APC) was read at 566, 620 and 652, respectively, using a portable spectrometer (DR 2700, Hach, US). The absorbance was also read at 750 nm, to correct the background interference [28]. Equations by Bennett and Bogorad [26] were used to quantify the concentrations of respective phycobilins. The Phycobilin concentration was the summation of PE, PC and APC. Protein (PN) in bEPS extracts and bulk liquid fractions was measured using the modified Lowry method [29] with bovine serum albumin as standard. Whereas, polysaccharide (PS) in extracted bEPS and bulk liquid fractions was measured using the phenol-sulfuric method [30] with glucose as standard. Dissolved organic carbon (DOC) in different bulk liquid fractions was determined using a TOC analyzer (TOC-VCPH, Shimadzu, U.S.A). Dissolved oxygen in the reactor was measured using a portable DO probe (Orion star A223, Thermo Scientific). Bright light and auto-fluorescence microscopy (EVOS FL Color, AMEFC4300) were also performed on the produced OPGs to study changes in the microbial community, especially cyanobacteria, and the overall structural development.

2.4. Statistical analysis

Pearson correlation coefficient and p-value analyses were conducted using the Pearson and two-sample t-test, respectively, in Microsoft Excel 2019 to compute correlations and significance between the experimental variables.

3. Results and discussion

3.1. Progression of photogranulation in hydrodynamic batches

The transformation of activated sludge flocs into OPGs in hydrodynamic batches is illustrated in Fig. 1. The floc size increased with negligible phototrophic growth during the first two to three days of the incubation period. These aggregates were enriched with filamentous bacteria, which seemed to serve as their backbone. By Day 4, the increase in floc size was accompanied by phototrophic growth, which included filamentous cyanobacteria (indicated by imposed autofluorescence) (Fig. 1 C, I). The abundance of filamentous cyanobacteria was significantly less than microalgae (both filamentous and unicellular forms) during Days 4–12). Cyanobacteria became the dominant phototrophic community in aggregates after Day 12. The growth of filamentous cyanobacteria has been established as a key driver for the formation of OPGs [1,4,19] Indeed, the continued growth of filamentous cyanobacteria in the aggregates prompted the formation of sphere-like OPGs (size range up to 1–2 mm) by Day 17–19 (Fig. 1E, K). The produced OPGs were enriched with filamentous cyanobacteria which existed throughout the photogranular biomass as seen with autofluorescence microscopy (Fig. 1 F, L). Abouhend et al. [1] also made similar microscopic observations with OPGs produced in bioreactors with diameters of 2 mm or less.

In terms of biomass concentration, Amherst and Hadley activated sludge inoculums had an average total solids (TS) concentration of 1300 ± 205 mg/L and 1573 ± 175 mg/L, respectively (Fig. 2A, B). TS concentration showed a decline during the first two days, attributable to the sludge degradation, after which it started to recover and reached a plateau for the remaining course of cultivation. The VS/TS ratio was steady throughout the cultivation period with average values of 0.77 ± 0.03 (Amherst) and 0.74 ± 0.06 (Hadley).

The photopigment analysis was conducted to understand the extent of phototrophic growth in the hydrodynamic batches as presented in Fig. 3. Chlorophyll a and b showed negligible production during Days 0–3, which afterwards increased in both cultivation sets (Fig. 3 A, B). Green algae produced both chlorophyll a and b whereas cyanobacteria produced only chlorophyll a. Continued increase in chlorophyll a and b during Days 15–19 suggests enhanced growth of microalgae. It should be noted that the solids concentration and VS/TS ratio during Days 15–19 was steady as observed in Fig. 2. This potentially suggests bacterial cell lysis, which would support microalgal growth since their growth rate is faster than cyanobacteria.

Besides chlorophyll a and b, chlorophyll c showed a gradual increase

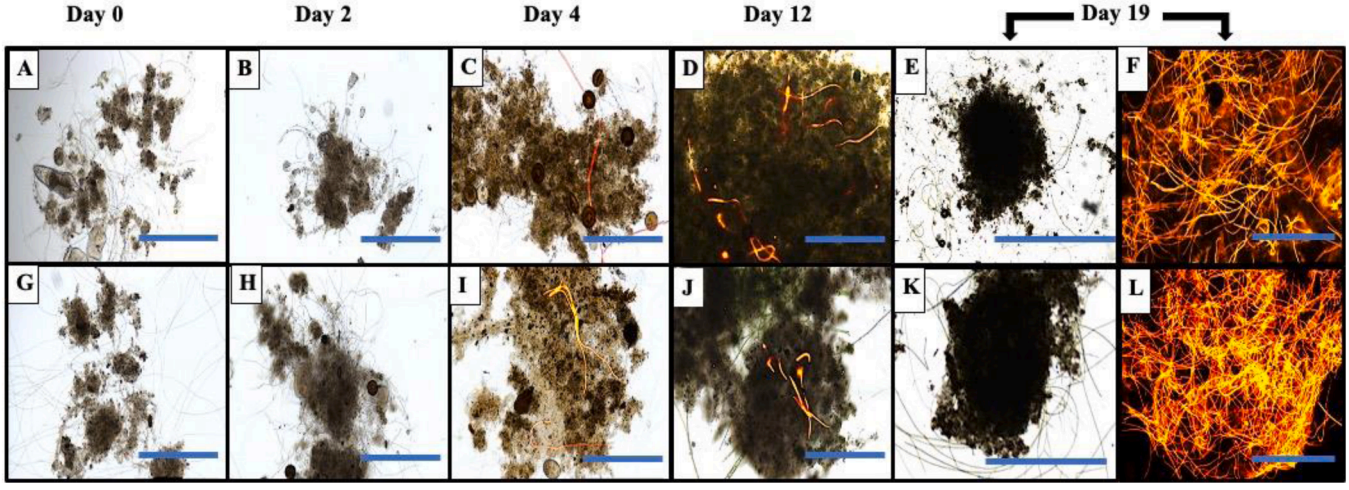

Fig. 1. Microscopic observation depicting the progression of photogranulation under hydrodynamic batch conditions using Amherst (A-F) and Hadley (G-L) activated sludges. Panels E and K have a scale bar of 2000 μm, while the rest have a scale bar of 400 μm.

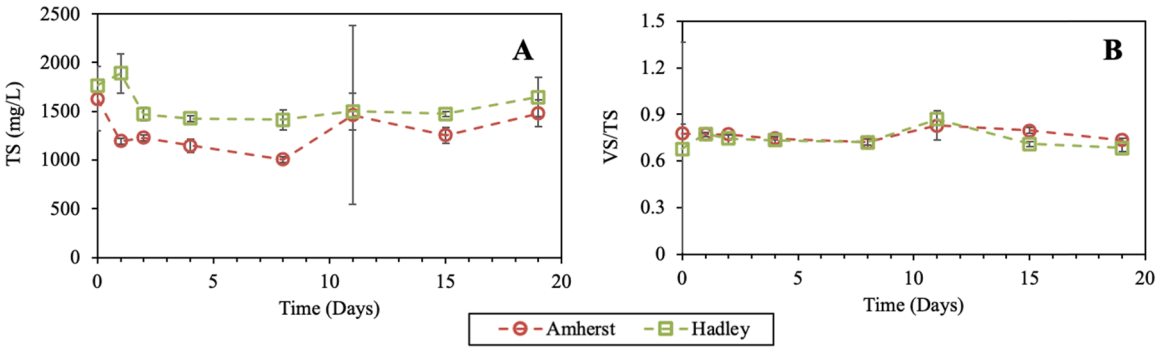

Fig. 2. Changes in the (A) total solids concentration (TS, mg/L) and (B) volatile solids/ total solids ratio (VS/TS) during the progression of photogranulation under hydrodynamic batch conditions. Error bars represent standard deviation from triplicate samples.

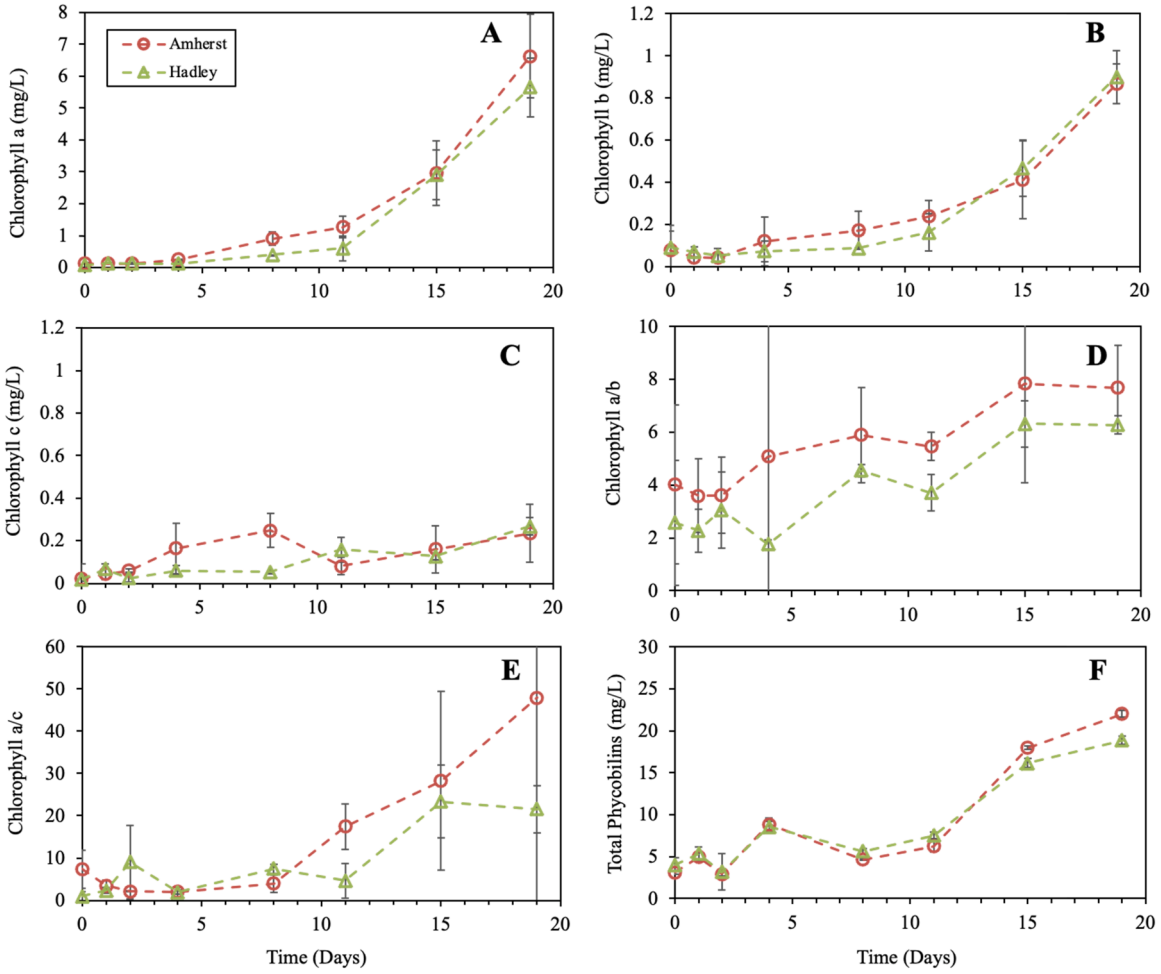

Fig. 3. Production of photo-pigment (A) chlorophyll a, (B) chlorophyll b, (C) chlorophyll c, (D) chlorophyll a/b, (E) chlorophyll a/c, and (F) phycobilin during the photogranulation process under hydrodynamic batch conditions. Error bars represent standard deviation from triplicate samples.

over the course of cultivation as presented in Fig. 3 C. The production of chlorophyll c suggested the growth of diatoms in the system, which was confirmed through microscopic observation. Chlorophyll a/b and a/c ratios were used to understand the growth of cyanobacteria with respect to green algae and diatoms, respectively (Fig. 3D, E). The Hadley set showed an increase in chlorophyll a/b and a/c ratios over time, which reached a plateau during Days 15–19. Likewise, the Amherst batch set showed overall similar trends for chlorophyll a/b and a/c.

Phycobilin, an accessory pigment in cyanobacteria, was also used as an indicator for cyanobacterial growth (Fig. 3F). Initially, phycobilin content showed a gradual increase till Day 12, which later increased sharply till Day 15. Phycobilin content is expected to have eventually reached stable levels during Days 15–19 since mature OPGs appear once cyanobacteria stop growing [5,9]. These findings indicate that cyanobacteria continued to grow till Day 15 after which they reached the stationary phase and tended to aggregate into the photogranular structure by Day 19. A strong positive correlation existed between chlorophyll a and phycobilin for Amherst ($r = 0.92$) and Hadley ($r = 0.93$) sets. Likewise, a strong positive correlation existed between chlorophyll a/b and phycobilin ($r = 0.89$ Amherst; $r = 0.80$ Hadley), and

chlorophyll a/c and phycobilin (r = 0.91 Amherst; r = 0.86 Hadley). Overall, these results indicate that hydrodynamic batches followed a similar photogranulation phenomenon as hydrostatic cultivation [9], i.e., the formation of OPGs is accompanied with the growth of phototrophs, especially cyanobacteria, which eventually reach the stationary growth phase.

3.2. Fate and dynamics of bulk-liquid Fe in hydrodynamic batches

Both Amherst and Hadley activated sludge inoculums showed initial Fe concentrations of 0.280 ± 0.002 mg/L and 0.010 ± 0.007 mg/L in dissolved and colloidal bulk liquid fractions, respectively. Upon incubation, a sharp release of Fe occurred in both cultivation sets. In the Amherst cultivation, the dissolved and colloidal Fe fraction increased to 0.320 ± 0.002 mg/L and 0.111 ± 0.064 mg/L, respectively, by Day 0.5 (Fig. 4 A-D). Whereas the counterparts in the Hadley set increased to 0.309 ± 0.004 mg/L and 0.071 ± 0.043 mg/L by Day 0.83 respectively (Fig. 4 G-J). The sharp release of Fe(II) should be via photochemical reduction of Fe(III) to Fe(II) [31,32] and also via the development of anaerobic conditions resulting from enhanced abiotic and biotic reactions consuming O_2 (Fig. 4 E-F, K-L). Strong negative correlations were found between the total bulk-liquid Fe(II) and DO (Amherst, r = −0.84; Hadley, r = −0.80). Among the two size fractions, dissolved Fe(II) showed stronger negative correlations with DO (Amherst, r = −0.89; Hadley, r = −0.80) compared to colloidal Fe(II) (Amherst, r = −0.43; Hadley, r = −0.49). Besides Fe(II), Fe(III) was also present in the bulk liquids during this early batch period.

After the release, the bulk-liquid Fe started to decrease till Day 2–3, after which it reached steady levels in both size fractions by Day 11 in Amherst and Day 8 in Hadley. Fe(II) was the dominant redox state in the bulk liquids during the first three days of incubation. However, it decreased in both bulk liquid size fractions, which should be due to microbial uptake or reoxidation into Fe(III) and both could be coupled with the growth of phototrophs and the production of O_2. Indeed, the decline in Fe(II) seemed to occur simultaneously with the increase in Fe (III) till Day 11, after which both Fe oxidation states reached a plateau.

Slight decreases in dissolved Fe concentrations occurred simultaneously with increases in colloidal Fe during Days 11–15 in Amherst and Days 8–15 in Hadley cultivations. During this period (Days 8–19), strong positive correlations were observed between colloidal Fe and soluble EPS (Amherst, r = 0.90; Hadley, r = 0.85). This shows that the released soluble EPS can potentially form complexes with a fraction of the dissolved Fe pool, thereby producing an organically complex colloidal Fe. Regardless of the shift in Fe size distribution, the total bulk-liquid content remained relatively constant during this time period.

The progression of photogranulation was accompanied by the release of DOC in both dissolved and colloidal bulk liquid fractions as presented in Fig. 5A, B. According to the research literature, Fe(III) complexed with organic ligands at a low Fe/ligand ratio needs to undergo biological and/or photochemical reduction for effective uptake [33]. In contrast, a high Fe/ligand condition induces a rapid exchange and production of unchelated Fe(III) from Fe(III)-ligand complex [34]. In this study, the Fe/DOC ratio in the dissolved fraction continued to decrease till Day 11 before reaching stable values (Fig. 5C-D). This Fe/DOC ratio was also very low throughout the batch period with 0.04 ± 0.02 and 0.04 ± 0.01 in Amherst and Hadley, respectively. Likewise, low Fe/DOC ratios for the colloidal fraction existed in Amherst (0.005 ± 0.004) and Hadley (0.01 ± 0.01) cultivation during the entire batch period. These results imply that the availability of bulk-liquid Fe was negatively impacted by the release of DOC, including soluble EPS, during the progression of photogranulation under hydrodynamic batches. These findings, along with the trends in bulk-liquid Fe size and oxidation state distribution, are similar to the previously reported hydrostatic cultivation study [9].

Table 1 presents the correlation coefficients between different fractions of soluble EPS and bulk-liquid Fe. Soluble EPS exhibited negative correlations with dissolved total Fe and Fe(II). The correlations were stronger for dissolved Fe(II) and EPS PS (Amherst, r = −0.91; Hadley, r = −0.61) than EPS PN (Amherst, r = −0.59; Hadley, r = −0.53). Soluble EPS also showed positive correlations with colloidal Fe(III) and total colloidal Fe. These findings are, again, similar to the results of a hydrostatic batch study [9].

Pearson correlation analysis was also conducted between the bulk-liquid Fe and the produced photo-pigments (Table 1). Phototrophic growth, indicated by pigment production, showed a higher dependence on the dissolved Fe pool as compared to the colloidal Fe pool due to a higher negative correlation. According to the literature, Fe pool in the aquatic environment consists of particulate, colloidal, and dissolved forms, with the dissolved fraction being the most available [35]. Within the dissolved pool, only Fe(II) exhibited a strong negative correlation with pigments, which indicates that dissolved Fe(II) was the preferred form of Fe for phototrophic growth. The colloidal Fe(II) pool, on the other hand, showed a weak to moderate negative correlation with the produced pigments. The analysis also revealed a competitive environment between the different phototrophic communities for the consumption of bulk-liquid Fe(II). Among phototrophs, cyanobacteria and diatoms exhibited the highest negative correlation with both dissolved and colloidal Fe(II) as compared to microalgae. This finding is different from the earlier hydrostatic study which showed eukaryotic microalgae having a comparatively stronger negative correlation with bulk-liquid Fe as compared to cyanobacteria and/or diatom [9,32].

3.3. Interaction between bEPS and Fe

The relationship between bEPS fractions and its associated Fe content is presented in Fig. 6. During Days 0–4, the bEPS protein (PN) declined sharply from 150.9 ± 8.8 mg/L to 80.9 ± 15.6 mg/L in Amherst and from 122.6 ± 7.2 mg/L to 76.4 ± 7.0 mg/L in Hadley. Significant degradation of bEPS-PN under anaerobic conditions has been reported to initiate the photogranulation process under a hydrostatic environment [5,9]. The bEPS-PN content continued to decrease till Day 11 in both sludges, with a higher degradation observed in Hadley as compared to Amherst. Afterwards, the bEPS-PN reached steady levels in Amherst, while Hadley showed a slight increase and then a decline during Days 11–19. Overall, the bEPS-PN content decreased up to 64.1 ± 3.7 % in Amherst and 76.0 ± 0.1 % in Hadley during the progression of photogranulation. These trends are consistent with earlier bEPS-PN observations during the photogranulation process in a hydrostatic environment [5,9].

Fig. 6 also shows similar trends between bEPS-Fe and bEPS-PN during the photogranulation process. Indeed, the Pearson correlation showed strong positive correlations between bEPS-Fe and bEPS-PN (Amherst, r = 0.93; Hadley, r = 0.96). According to the literature, Fe mostly resides within the sludge biomass matrix due to its strong affinity with EPS protein, [36] which is the major component of the activated sludge EPS [37]. Previous studies have postulated that the large release of proteins occurring under anaerobic conditions is due to the reduction of Fe [36,38]. This suggests that the release of Fe(II) into the bulk liquid fractions (Fig. 4) under anaerobic conditions occurred due to the degradation of activated sludge. The results also illustrate that bEPS-PN was the major source of accessible Fe pool as it continued to decline along with the progression of photogranulation. The bEPS-Fe content eventually reached steady levels by Day 11. During the later stages of cultivation, the cyanobacterial growth (as indicated by phycobilin, chlorophyll a/b, chlorophyll a/c) seemed to reach a stationary growth phase and OPGs appeared. These findings further signify the similarity between hydrostatic and hydrodynamic batch conditions since we observed OPGs appearing around the time the bEPS-Fe pool reached stable levels in hydrostatic conditions [9].

Unlike protein, bEPS-PS initially increased from Day 0–2 in both sludges thereby yielding a moderate to strong negative correlation with bEPS-Fe (Amherst, r = −0.58; Hadley, r = −0.85). Afterwards, bEPS-PS declined and appeared to reach steady levels for the remainder of the

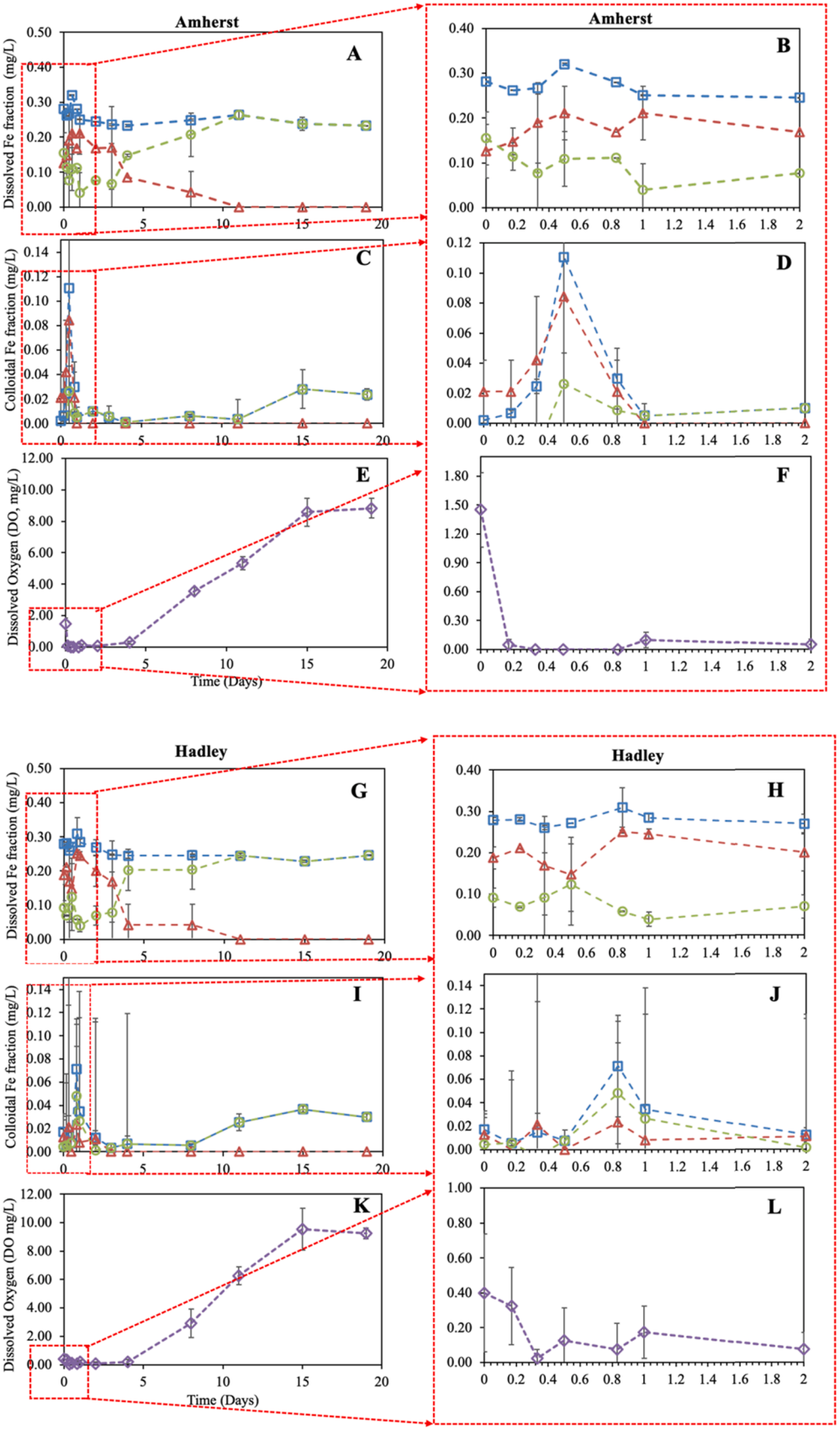

Fig. 4. Fate of Fe in different bulk liquid size fractions in Amherst (A-D) and Hadley (G-J) during the hydrodynamic cultivation. Panels E and K depict the changes in dissolved oxygen (DO, mg/L), while panels B, D, F, H, J and L represent the zoomed data sets during Day 0–2. Error bars represent the range of results from duplicate samples.

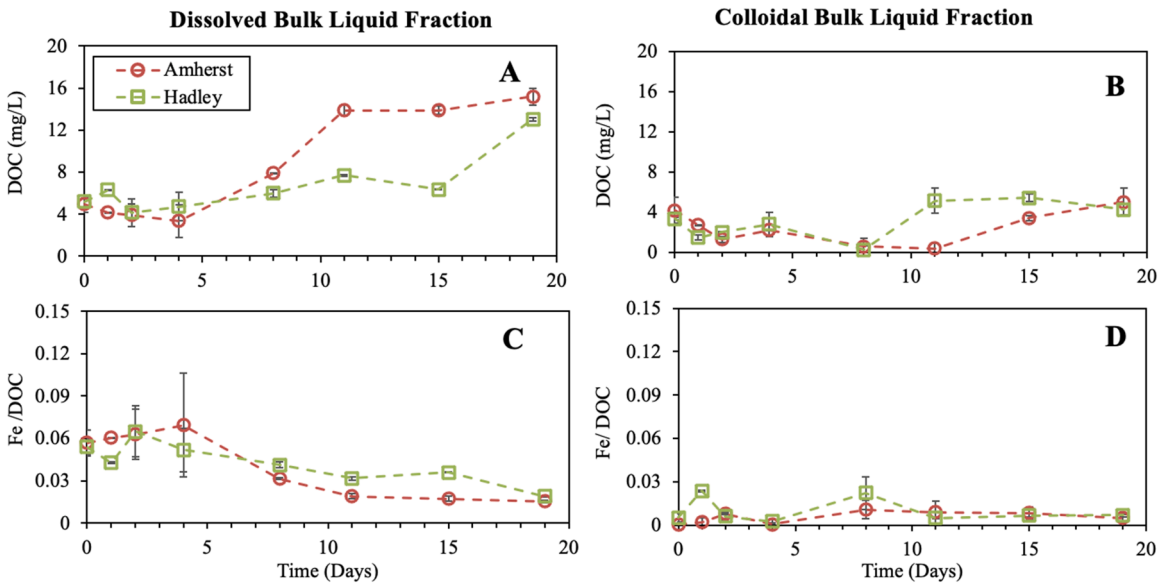

Fig. 5. Dissolved organic carbon (DOC) and Fe/DOC ratio in dissolved (A, C) and colloidal (B, D) bulk liquid fractions.

Table 1
Pearson correlation analysis of bulk-liquid Fe fractions with produced photo-pigments and extracellular polymeric substances (EPS).

		Dissolved Fe (Fe < 30 kDa)			Collodial Fe (30 kDa < Fe < 0.45 μm)		
Amherst		Total Fe	Fe (II)	Fe (III)	Total	Fe (II)	Fe (III)
Soluble EPS	Protein (PN)	-0.25	-0.59	0.55	0.32	-0.42	0.45
	Polysaccharide (PS)	-0.22	-0.91	0.89	0.91	-0.27	0.79
	PS/PN	-0.12	-0.81	0.81	0.53	-0.13	0.44
Pigments	Phycobilin	-0.62	-0.65	0.54	0.85	-0.32	0.77
	Chlorophyll a	-0.47	-0.65	0.58	0.79	-0.25	0.69
	Chlorophyll b	-0.46	-0.70	0.62	0.76	-0.24	0.67
	Chlorophyll c	-0.66	-0.67	0.55	0.45	-0.49	0.57
	Chlorophyll a/b	-0.50	-0.88	0.81	0.79	-0.33	0.73
	Chlorophyll a/c	-0.34	-0.69	0.64	0.80	-0.16	0.65
Hadley		Total Fe	Fe (II)	Fe (III)	Total	Fe (II)	Fe (III)
Soluble EPS	Protein (PN)	-0.60	-0.53	0.50	0.27	-0.21	0.32
	Polysaccharide (PS)	-0.55	-0.61	0.62	-0.02	-0.41	0.15
	PS/PN	0.15	-0.03	0.08	0.34	-0.04	0.32
Pigments	Phycobilin	-0.68	-0.70	0.69	0.55	-0.64	0.75
	Chlorophyll a	-0.49	-0.55	0.56	0.53	-0.46	0.65
	Chlorophyll b	-0.47	-0.55	0.56	0.53	-0.45	0.65
	Chlorophyll c	-0.52	-0.66	0.68	0.55	-0.61	0.73
	Chlorophyll a/b	-0.66	-0.64	0.63	0.46	-0.53	0.62
	Chlorophyll a/c	-0.62	-0.54	0.51	0.50	-0.44	0.62

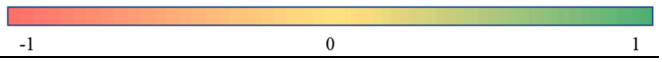

cultivation period. These changes resulted in a moderate to strong positive correlation with bEPS-Fe (Amherst, r = 0.37; Hadley, r = 0.92). The bEPS-PS results contradict the earlier hydrostatic observations where bEPS-PS and bEPS-Fe exhibited moderate to strong negative correlations during the progression of photogranulation [9]. Fe can bind to EPS PS in the presence of a carboxylic group, especially uronic acids and is known to accumulate over the outer polysaccharide sheath of cyanobacteria [39,40]. It can be speculated that bEPS-PS might be another source of Fe in hydrodynamic batches, though not as major as bEPS-PN.

To understand the extent of the phototrophic dependence on the bEPS-Fe pool during the photogranulation process, a further correlation analysis was conducted between bEPS-Fe and various photosynthetic pigments (Table 2). Phycobilin showed moderately stronger correlations with bEPS-Fe (Amherst, r = −0.68; Hadley, r = −0.66) as compared to chlorophyll a (Amherst, r = −0.56; Hadley, r = −0.55) and chlorophyll b (Amherst, r = −0.60; Hadley, r = −0.55). Likewise, chlorophyll a/b and a/c were found to exhibit stronger correlations with bEPS-Fe than chlorophyll a and b in Hadley. These results suggest that cyanobacteria are more dependent on the bEPS-Fe pool than microalgae. Besides cyanobacteria, a moderate correlation between chlorophyll c and bEPS-Fe also implied the reliance of diatoms on bEPS-Fe. These results are quite similar to those for bulk-liquid Fe in this study, which suggests that cyanobacteria and diatoms both thrive on bEPS-Fe and dissolved Fe(II) pool under hydrodynamic operation. Previously, we conveyed cyanobacteria depended mostly on bEPS-Fe for growth under hydrostatic cultivation [9].

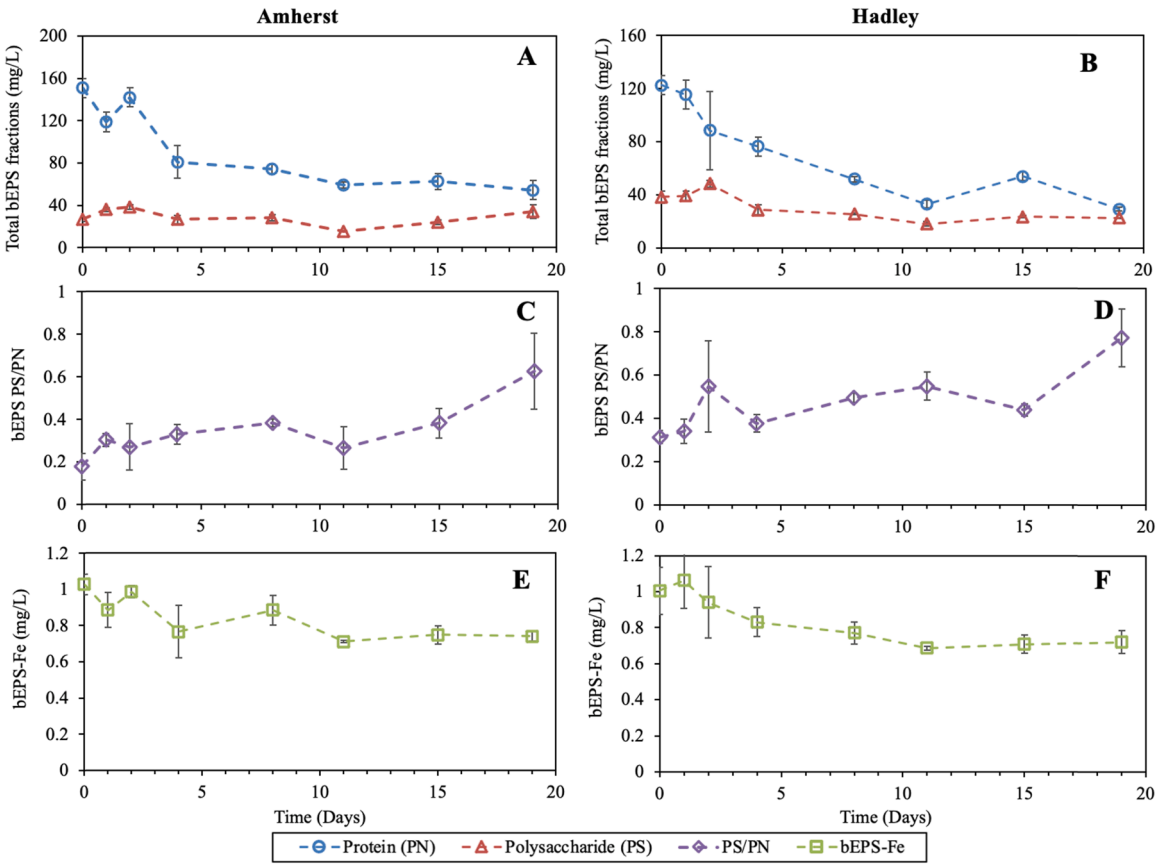

Fig. 6. Changes in extracted biomass-bound extracellular polymeric substances (bEPS, mg/L) fractions (A-B) and their ratio (C-D) during the progression of photogranulation under hydrodynamic batch cultivation. The figure also displays the relationship of bEPS with bEPS associated Fe pool (bEPS-Fe, mg/L) (E-F) over the course of cultivation. Error bars represent standard deviation from triplicate samples.

Table 2
Heatmap representing the Pearson correlation coefficients of bEPS-Fe with produced pigments and different fractions of bEPS during the hydrodynamic batch cultivation.

		Amherst	Hadley
Bound EPS	Protein (PN)	0.93	0.96
	Polysaccharide (PS)	0.50	0.87
	Humics	0.87	0.98
	PS/PN	-0.56	-0.61
Pigments	Phycobilin	-0.68	-0.66
	Chlorophyll a	-0.56	-0.55
	Chlorophyll b	-0.60	-0.55
	Chlorophyll c	-0.52	-0.67
	Chlorophyll a/b	-0.72	-0.71
	Chlorophyll a/c	-0.59	-0.60

-1 0 1

3.4. Distribution of Fe in the photogranular system

The average whole biomass Fe of 9.4 ± 0.5 mg/L and 10.3 ± 1.3 mg/L was found in Amherst and Hadley activated sludges, respectively. At the time of incubation, Fe content was highest in the pellet fraction (Amherst, 86 %; Hadley, 88 %), followed by the bEPS extract (Amherst, 11 %; Hadley, 9 %) and bulk liquid (Amherst, 3 %; Hadley, 3 %) (Fig. 7). The pellet Fe content continued to increase over the course of cultivation, reaching up to 89 % in Amherst and 90 % in Hadley by Day 19. Contrarily, bEPS-Fe decreased by 3 % in Amherst and 2 % in Hadley. The bulk-liquid Fe decreased by only 0.3 % in both cultivation sets during the entire cultivation period. Both the bulk liquid

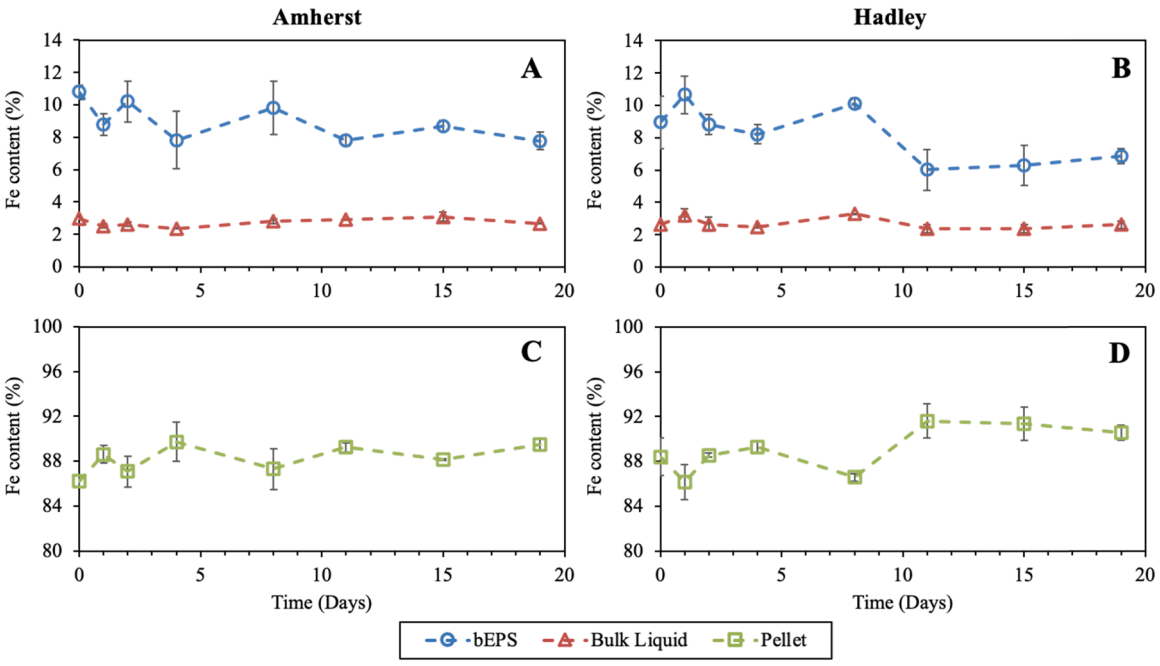

Fig. 7. Distribution of Fe (%) in different fractions of photogranular biomass over the course of cultivation. Error bars represent the range of results in duplicate samples.

and bEPS-Fe fractions seemed to reach steady levels during Days 11–19. Overall, the Fe distribution was similar between the activated sludge and photogranular biomass, i.e., pellet Fe > > bEPS-Fe > bulk-liquid Fe. These Fe distribution trends were also found statistically similar across the two sludges ($p < 0.66$).

The previous hydrostatic cultivation study revealed a similar Fe distribution trend across the cultivation period [9]. However, the extent of Fe reduction in the bEPS extract and the bulk liquid was much greater under hydrostatic conditions compared to the current hydrodynamic batches. Ansari et al. [9] reported the bEPS-Fe content decreased from 7.6 ± 1.5 % to 1.3 ± 0.2 %, while the bulk-liquid Fe decreased from 5.2 ± 1.9 % to 0.8 ± 0.2 % during the photogranulation process under hydrostatic conditions. Oxic environments promote the formation of insoluble Fe(III) precipitates, especially Fe(III) oxides in aquatic systems. The literature also shows that Fe in oxic aquatic environments mostly exists in Fe (III)-organic complex and Fe(III) oxide form, with the latter up to 60 %, in the supernatant of activated sludge membrane bioreactor [41]. It is possible that due to the presence of shear, the rate

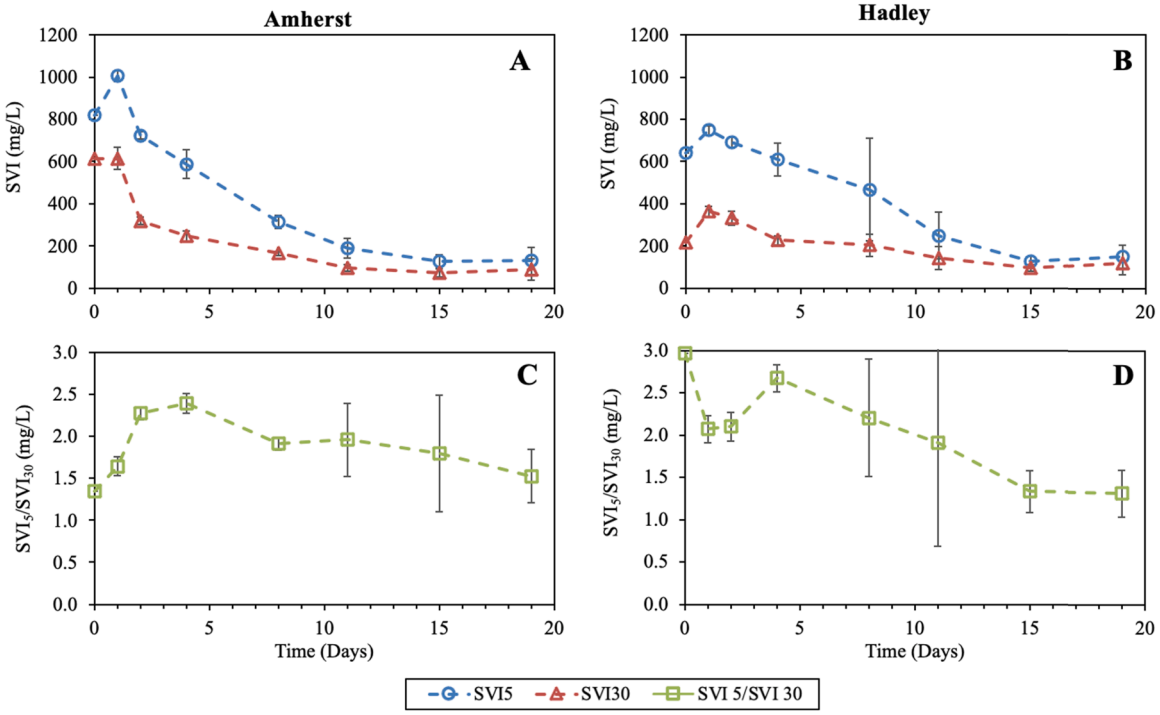

Fig. 8. Impact on biomass settleability as measured by sludge volume index after 5 mins (SVI_5) and 30 mins (SVI_{30}) (A-B). Impact on SVI_5/SVI_{30} ratio during the progression of photogranules is also depicted in figure C-D. Error bars represent the range of results from quadruple samples.

of binding of newly formed Fe(III)-organic complexes or precipitates to bEPS is greater than the rate of consumption of bEPS associated Fe(III) pool, thereby impacting the accessibility of Fe. This might suggest why utilization (decrease) of Fe in both the bulk liquid and bEPS fractions is not as high as that seen in hydrostatic cultivation.

3.5. Biomass settleability and Fe

The sludge volume index (SVI, mL/g) was determined to understand the impact on biomass settleability during the photogranulation process (Fig. 8(A-B)). The mixed photogranular biomass in Amherst showed a decreasing SVI over the course of cultivation. It decreased to 129 ± 64 and 89 ± 50 mL/g after 5 min and 30 min of settling time, respectively, by the end of the cultivation period. No statistical difference was seen between the SVI_5 and SVI_{30} trends of the Amherst system ($p < 0.18$). Decreasing SVI_5 and SVI_{30} trends also occurred in Hadley, and they were statistically different from each other ($p < 0.03$). The undiluted activated sludge, which was collected from the WWTP for the batch operation, showed SVI_{30} in the range of 315–375 mL/g and 215–300 mL/g in Amherst and Hadley, respectively. This shows that produced photogranular biomass has much greater settleability compared to their activated sludge inoculums.

The extent of OPG formation was also investigated by analyzing the SVI_5/SVI_{30} ratio (Fig. 8 (C-D)). According to the literature, granule-based systems exhibit an SVI_5/SVI_{30} ratio nearer to 1 since approximately all of the granular biomass settle by 5 min [42]. The SVI_5/SVI_{30} initially increased from 1.3 to 2.4 in Amherst during Days 0–4. In contrast, Hadley showed an initial decrease from 3 to 2.1 and later an increase up to 2.7 by Day 4. This increasing SVI_5/SVI_{30} ratio is due to the higher rate of activated sludge degradation than the photogranulation during this time period. The SVI_5/SVI_{30} ratio started to decrease from Day 4 onwards reaching ratios as low as 1.5 and 1.3 in Amherst and Hadley, respectively. These results support the earlier microscopic observations that depict the increase in size and formation of OPGs after Day 4 in both Amherst and Hadley batches.

The relationships between the Fe content and biomass settleability were then examined (Table 3). The bEPS-Fe pool exhibited strong positive correlations with both SVI_5 (Amherst, $r = 0.74$; Hadley, $r = 0.89$) and SVI_{30} (Amherst, $r = 0.76$; Hadley, $r = 0.86$) during the course of batch operation. During the same time period, the dissolved bulk-liquid Fe showed moderate to strong positive correlations with SVI_5 (Amherst, $r = 0.36$; Hadley, $r = 0.82$) and SVI_{30} (Amherst, $r = 0.55$; Hadley, $r = 0.82$). These findings reflect comparatively weaker correlation strength between dissolved bulk-liquid Fe and SVI in contrast to bEPS-Fe and SVI. The positive correlations between the bEPS-Fe pool and SVI indicate a strong influence of phototrophic growth, especially cyanobacteria, on the promotion of granular settleability. The SVI_5/SVI_{30} ratio also showed a moderately positive correlation with different Fe fractions in Hadley. The correlation between SVI_5/SVI_{30} and bEPS-Fe and dissolved Fe became positive in Amherst from Day 8 onwards (bEPS-Fe, $r = 0.25$; Dissolved Fe, $r = 0.87$).

Unlike bEPS-Fe and the dissolved bulk-liquid Fe, the colloidal bulk-liquid Fe pool showed weak to moderate negative correlations with both SVI_5 (Amherst, $r = -0.60$; Hadley, $r = -0.46$) and SVI_{30} (Amherst, $r = -0.54$; Hadley, $r = -0.25$). Besides the colloidal pool, pellet Fe fraction also exhibited negative correlations with SVI_5 (Amherst, $r = -0.38$; Hadley, $r = -0.78$) and SVI_{30} (Amherst, $r = -0.47$; Hadley, $r = -0.77$) during the course of photogranulation. According to Juang et al. [43], the accumulation of Fe precipitates (in the form of Fe phosphates and oxides) in the granule leads to enhanced structural stability. Other studies have also reported that the presence of Fe precipitates increased the size, stability, and settling velocities of aerobic and anaerobic granules [44,45]. It was observed that the presence of Fe (III) oxides/oxyhydroxides in hydrostatic cultivation mostly resided within the photogranular biomass [9]. In this study, the oxic environment is also expected to encourage the formation of Fe(III) oxide, which will continue to accumulate in photogranular biomass over time and promote biomass settleability. The biomass-bound EPS PS/PN also demonstrated a negative correlation with SVI_5 (Amherst, $r = -0.61$; Hadley, $r = -0.62$) and SVI_{30} (Amherst, $r = -0.59$; Hadley, $r = -0.42$). Overall, these results imply that the photogranular stability in hydrodynamic batches is dependent upon the growth of the cyanobacterial community and the presence of potential Fe precipitates within the formed OPGs.

4. Conclusions

From the initial incubation of activated sludge to the formation of OPGs, this study presents how the fate and dynamics of Fe may influence the progression of photogranulation under the hydrodynamic batch conditions. A sharp Fe release in the bulk liquid was associated with the earlier development of anaerobic conditions. This released Fe rapidly decreased and reached steady levels of 0.261 ± 0.006 and 0.265 ± 0.011 mg/L in Amherst and Hadley, respectively, during the last stages of cultivation. The fate and dynamics of Fe oxidation states [Fe(II) and Fe(III)] as well as the size fraction of bulk liquid Fe (dissolved and colloidal) also seemed to impact the photogranulation with dissolved Fe (II) being the limiting available Fe. Moreover, the Fe/DOC ratios decreased in the bulk liquid fractions to the average of 0.042 ± 0.001 (dissolved) and 0.0075 ± 0.0025 (colloidal), which is known to impact the availability of Fe. Besides bulk liquid Fe, the extracted bEPS-Fe pool decreased by more than 70 % in both sludges, after which it reached a plateau and OPGs started to appear. A strong negative correlation existed between bEPS-Fe and phototrophic growth especially

Table 3
Heatmap depicting the Pearson correlation analysis of sludge settling index (SVI) with different Fe fractions.

			Bulk-Liquid	
		bEPS-Fe	Dissolved Fe	Colloidal Fe
SVI_5	Amherst	0.74	0.36	-0.60
	Hadley	0.89	0.82	-0.46
SVI_{30}	Amherst	0.76	0.55	-0.54
	Hadley	0.86	0.82	-0.25
SVI_5/SVI_{30}	Amherst	-0.19	-0.48	-0.24
	Hadley	0.60	0.54	-0.67

-1 0 1

cyanobacteria. Finally, the highest Fe content resided in the pellet fraction (~ 90 %), followed by the extracted bEPS (~ 8 %) and bulk liquid (~ 2 %) in the photogranular system. These findings exhibit similarities in the photogranulation phenomenon between the batch hydrodynamic and the previously reported hydrostatic cultivation. It can, therefore, be concluded that the progression of photogranulation is accompanied with the growing limitation of available Fe pool irrespective of static or hydrodynamic cultivation conditions.

It will be interesting to examine in future studies how pellet Fe fraction changes with an increase in photogranular size. Future studies can also focus on ecology, genomic and proteomics analysis to better understand the distribution/abundance of microbial communities in batch hydrodynamically-produced OPGs, the genes associated with Fe storage and limitation, and whether these protein expressions are active or not, respectively. The current study establishes Fe as a major player in influencing cyanobacterial physiology and ultimately the formation of photogranulation. Continued investigations on the role of Fe are expected to enhance our fundamental knowledge of the photogranulation phenomenon. The acquired knowledge will make a significant contribution in promoting the successful production of OPGs and the design of an effective OPG-based wastewater treatment technology.

Declaration

The authors declare no competing financial interest.

CRediT authorship contribution statement

Abeera A. Ansari: Experimentation, Data collection, Writing – original draft, Conceptualization, Validation, Writing – review & editing, Methodology, Writing – original draft, Supervision. Arfa A. Ansari: Experimentation, Data collection, Writing – original draft**. Asif Hussain Khoja:** Experimentation, Data collection, Writing – original draft preparation, Data validation, Writing – review & editing references. **Ahmed S. Abouhend:** Conceptualization, Methodology, Writing – original draft, Supervision. **Chul Park:** Conceptualization, Methodology, Writing – original draft, Supervision, Writing – editing and proofing of manuscript.

Declaration of Competing Interest

The authors declare that they have no known competing financial interests or personal relationships that could have appeared to influence the work reported in this paper.

Data Availability

No data was used for the research described in the article.

Acknowledgement

The authors would like to thank Dr. Dhandapani Venkataraman and Dr. Kevin Kittilstved for providing laboratory facilities in the Department of Chemistry at UMass Amherst. The authors also thank Mohammad Abdullah and Andrew Keyser for insightful comments and suggestions during the study. This work was supported by the grants from the National Science Foundation (CBET1605424; IIP1919091) and the National University of Sciences and Technology, Pakistan.

References

[1] A.S. Abouhend, A. McNair, W.C. Kuo-Dahab, C. Watt, C.S. Butler, K. Milferstedt, J. Hamelin, J. Seo, K.M. El-moselhy, C. Park, The oxygenic photogranule process for wastewater treatment, Environ. Sci. Technol. 52 (2018) 3503–3511, https://doi.org/10.1021/acs.est.8b00403.

[2] A.S. Abouhend, K. Milferstedt, J. Hamelin, A.A. Ansari, C. Butler, B.I. Carbajal-González, C. Park, Growth progression of oxygenic photogranules and its impact on bioactivity for aeration-free wastewater treatment, Environ. Sci. Technol. 54 (2020) 486–496, https://doi.org/10.1021/acs.est.9b04745.

[3] J.L. Campos, D. Valenzuela-Heredia, A. Pedrouso, A. Val del Río, M. Belmonte, A. Mosquera-Corral, Greenhouse gases emissions from wastewater treatment plants: minimization, treatment, and prevention, J. Chem. 2016 (2016), 3796352, https://doi.org/10.1155/2016/3796352.

[4] K. Milferstedt, W.C. Kuo-Dahab, C.S. Butler, J. Hamelin, A.S. Abouhend, K. Stauch-White, A. McNair, C. Watt, B.I. Carbajal-González, S. Dolan, C. Park, The importance of filamentous cyanobacteria in the development of unusual oxygenic photogranules, Sci. Rep. 7 (2017) 1–15.

[5] W.C. Kuo-Dahab, K. Stauch-White, C. Butler, G.J. Gikonyo, B. Carbajal-Gonzalez, A. Ivanova, S. Dolan, C. Park, Investigation of the fate and dynamics of extracellular polymeric substances (EPS) during sludge-based photogranulation under hydrostatic conditions, Environ. Sci. Technol. 52 (2018) 10462–10471.

[6] C. Park, S. Dolan, Algal-sludge granule for wastewater treatment and bioenergy feedstock generation, US Pat. 10 (189) (2019) 732.

[7] K. Stauch-White, V.N. Srinivasan, W.C. Kuo-Dahab, C. Park, C.S. Butler, The role of inorganic nitrogen in successful formation of granular biofilms for wastewater treatment that support cyanobacteria and bacteria, AMB Express 7 (2017), https://doi.org/10.1186/s13568-017-0444-8.

[8] A.A. Ansari, A.S. Abouhend, C. Park, Effects of seeding density on photogranulation and the start-up of the oxygenic photogranule process for aeration-free wastewater treatment, Algal Res. 40 (2019), 101495, https://doi.org/10.1016/j.algal.2019.101495.

[9] A.A. Ansari, A.A. Ansari, A.S. Abouhend, J.G. Gikonyo, C. Park, Photogranulation in a hydrostatic environment occurs with limitation of iron, Environ. Sci. Technol. 55 (2021) 10672–10683, https://doi.org/10.1021/acs.est.0c07374.

[10] J.G. Rueter, R.R. Petersen, Micronutrient effects on cyanobacterial growth and physiology, New Zeal.J. Mar. Freshw. Res. 21 (1987) 435–445.

[11] M. Fujii, T.C. Dang, A.L. Rose, T. Omura, T.D. Waite, Effect of light on iron uptake by the freshwater cyanobacterium microcystis aeruginosa, Environ. Sci. Technol. 45 (2011) 1391–1398, https://doi.org/10.1021/es103311h.

[12] H. Schoffman, H. Lis, Y. Shaked, N. Keren, T. Bibby, Iron – nutrient interactions within phytoplankton, Front. Plant Sci. 7 (2016) 1–12, https://doi.org/10.3389/fpls.2016.01223.

[13] J.A. Raven, Predictions of Mn and Fe use efficiencies of phototrophic growth as a function of light availability for growth and of c assimilation pathway, N. Phytol. 116 (1990) 1–18.

[14] L.E. Brand, Minimum iron requirements of marine phytoplankton and the implications for the biogeochemical control of new production, Limnol, Ocean 36 (1991) 1756–1771.

[15] A. Kustka, E.J. Carpenter, S.A. Sañudo-Wilhelmy, Iron and marine nitrogen fixation: progress and future directions, Res. Microbiol. 153 (2002) 255–262.

[16] H. Lis, C. Kranzler, N. Keren, Y. Shaked, A comparative study of iron uptake rates and mechanisms amongst marine and fresh water cyanobacteria: prevalence of reductive iron uptake, Life 5 (2015) 841–860, https://doi.org/10.3390/life5010841.

[17] B. Konczak, J. Karcz, K. Miksch, Influence of calcium, magnesium, and iron ions on aerobic granulation, Appl. Biochem. Biotechnol. 174 (2014) 2910–2918, https://doi.org/10.1007/s12010-014-1236-0.

[18] J.G. Gikonyo, A.A. Ansari, A. Abouhend, J.E. Tobiason, C. Park, Hydrodynamic granulation of oxygenic photogranules, Environ. Sci. Water Res. Technol. 7 (2021) 427–440.

[19] C. Park, N. Takeuchi, Unmasking photogranulation in decreasing glacial albedo and net autotrophic wastewater treatment, Environ. Microbiol. 23 (2021) 6391–6404.

[20] A.S. Abouhend, K. Milferstedt, J. Hamelin, A.A. Ansari, C. Butler, B.I. Carbajal-González, C. Park, Growth progression of oxygenic photogranules and its impact on bioactivity for aeration-free wastewater treatment, Environ. Sci. Technol. (2019), https://doi.org/10.1021/acs.est.9b04745.

[21] H.J.W. De Baar, J.T.M. DeJong, The Biogeochemistry of Iron in Seawater, Wiley,, Chichester, UK, 2001.

[22] C. Park, J.T. Novak, Characterization of activated sludge exocellular polymers using several cation-associated extraction methods, Water Res 41 (2007) 1679–1688, https://doi.org/10.1016/j.watres.2007.01.031.

[23] APHA. Standard methods for the examination of water and wastewater, twentysecond ed., American Public Health Association,, Washington D.C., USA, 2012.

[24] B.K. Pierson, M.N. Parenteau, B.M. Griffin, Phototrophs in high-iron-concentration microbial mats: physiological ecology of phototrophs in an iron-depositing hot spring, Appl. Environ. Microbiol. 65 (1999) 5474–5483.

[25] L.L. Stookey, Ferrozine—a new spectrophotometric reagent for iron, Anal. Chem. 42 (1970) 779–781, https://doi.org/10.1021/ac60289a016.

[26] A. Bennett, L. Bogorad, Complementary chromatic adaptation in a filamentous blue-green alga, J. Cell Biol. 58 (1973), 419 LP – 435, ⟨http://jcb.rupress.org/content/58/2/419.abstract⟩.

[27] A.M. Islam, J. Beardall, Growth and photosynthetic characteristics of toxic and non-toxic strains of the cyanobacteria microcystis aeruginosa and anabaena circinalis in relation to light, Microorg 5 (2017), https://doi.org/10.3390/microorganisms5030045.

[28] R. Lauceri, M. Bresciani, A. Lami, G. Morabito, Chlorophyll a interference in phycocyanin and allophycocyanin spectrophotometric quantification, J. Limnol. (2017), https://doi.org/10.4081/jlimnol.2017.

[29] F. Caccavo, B. Frolund, K. F, V. Ommen, P.H. Nielsen, Deflocculation of activated sludge by the dissimilatory Fe(III)-reducing bacterium shewanella alga BrY, Appl. Env. Microbiol 62 (1996) 1487–1490.

[30] M. DuBois, K.A. Gilles, J.K. Hamilton, P.A. Rebers, F. Smith, Colorimetric method for determination of sugars and related substances, Anal. Chem. 28 (1956) 350–356.
[31] M. Fujii, A.L. Rose, T. Omura, T.D. Waite, Effect of Fe(II) and Fe(III) transformation kinetics on iron acquisition by a toxic strain of Microcystis aeruginosa, Environ. Sci. Technol. 44 (2010) 1980–1986, https://doi.org/10.1021/es901315a.
[32] A.A. Ansari, Investigating the role of iron in the photogranulation phenomenon, University of Massachusetts, Amherst, USA, 2020.
[33] Q. Fu, M. Fujii, M. Natsuike, T.D. Waite, Iron uptake by bloom-forming freshwater cyanobacterium Microcystis aeruginosa in natural and effluent waters, Environ. Pollut. 247 (2019) 392–400, https://doi.org/10.1016/j.envpol.2019.01.071.
[34] M. Fujii, A. Imaoka, C. Yoshimura, T.D. Waite, Effects of molecular composition of natural organic matter on ferric iron complexation at circumneutral pH, Environ. Sci. Technol. 48 (2014) 4414–4424, https://doi.org/10.1021/es405496b.
[35] J.L. Martinez, Natural antibiotic resistance and contamination by antibiotic resistance determinants: the two ages in the evolution of resistance to antimicrobials, Front. Microbiol. 3 (2012), https://doi.org/10.3389/fmicb.2012.00001.
[36] J.T. Novak, M.E. Sadler, S.N. Murthy, Mechanisms of floc destruction during anaerobic and aerobic digestion and the effect on conditioning and dewatering of biosolids, Water Res 37 (2003) 3136–3144.
[37] P.H. Nielsen, A. Jahn, R. Palmgren, Conceptual model for production and composition of exopolymers in biofilms, Water Sci. Technol. 36 (1997) 11–19.
[38] C. Park, M.M. Abu-Orf, J.T. Novak, The digestibility of waste activated sludges, Water Environ. Res. 78 (2006) 59–68, https://doi.org/10.2175/106143005×84521.
[39] J. Bender, U. Rodriguezeaton, S. Ekanemesang, P. Phillips, Characterization of metal-binding bioflocculants produced by the cyanobacterial component of mixed microbial mats, Appl. Env. Microbiol 60 (1994) 2311–2315.
[40] B.A. Whitton (Ed.), Ecology of Cyanobacteria II: Their Diversity in Space and Time, Springer, Durham, UK, 2012, https://doi.org/10.1007/978-94-007-3855-3.
[41] X.M. Wang, T.D. Waite, Iron speciation and iron species transformation in activated sludge membrane bioreactors, Water Res 44 (2010) 3511–3521, https://doi.org/10.1016/j.watres.2010.03.031.
[42] M.C.M. van Loosdrecht, P.H. Nielsen, C.M. Lopez-Vazquez, D. Brdjanovic, Experimental Methods in Wastewater Treatment, IWA Publishing, 2016. ⟨https://books.google.com/books?id=k6rQDAAAQBAJ⟩.
[43] Y.C. Juang, S.S. Adav, D.J. Lee, J.H. Tay, Stable aerobic granules for continuous-flow reactors: precipitating calcium and iron salts in granular interiors, Bioresour. Technol. 101 (2010) 8051–8057, https://doi.org/10.1016/j.biortech.2010.05.078.
[44] G. Yilmaz, U. Bozkurt, K.A. Magden, Effect of iron ions (Fe2+, Fe3+) on the formation and structure of aerobic granular sludge, Biodegradation 28 (2017) 53–68, https://doi.org/10.1007/s10532-016-9777-2.
[45] A. Vlyssides, E.M. Barampouti, S. Mai, Influence of ferrous iron on the granularity of a UASB reactor, Chem. Eng. J. 146 (2009) 49–56, https://doi.org/10.1016/j.cej.2008.05.011.